BHM (2014) Vol. 159 (11): 447–453
DOI 10.1007/s00501-014-0304-7

BHM Berg- und Hüttenmännische Monatshefte

Change of Mold Slag Composition during Slab Casting of Steel with High Al Content

Harald Harmuth[1] and Guangmin Xia[2]

[1]Chair of Ceramics, Montanuniversitaet Leoben, Leoben, Austria
[2]voestalpine Stahl GmbH, Linz, Austria

Received August 20, 2014; accepted August 31, 2014; Published online October 24, 2014

Abstract: Three different mold slags have been sampled in dependence of time during slab casting of TRIP steel, and compositional changes have been analyzed. Mass transfer coefficients governing the decrease of silica and increase of alumina have been determined. Moreover change of manganese content was investigated in dependence of the initial manganese content of the mold powder which was close to zero for one of the powders investigated. The following findings have been revealed: Mass transfer coefficients are rising with increasing elapsed time or decreasing silica content, respectively. An initial increase of manganese content by oxidation from the steel followed by later reduction has been observed for the manganese free mold powder. For interpretation of these findings, further simulation according to an effective equilibrium reaction zone model was performed. It was revealed that the primary impact of the steel flow at the steel/slag interface close to the mold wall followed by a stratified flow is of major importance for the phenomena observed. Further results make it possible to predict the steady state composition and show that steady state silica content is nonzero in any case. Moreover, for the mold powders investigated here, it was concluded that manganese content does not decrease silica reduction.

Keywords: Mold slag, Silica reduction, Mass transfer coefficient

Änderung der Kokillenschlackenzusammensetzung beim Brammenstranggießen von Stahl mit hohem Al-Gehalt

Zusammenfassung: Die experimentell ermittelte Veränderung der chemischen Zusammensetzung von drei Gießschlacken beim Vergießen von TRIP Stahl diente als Grundlage zur Bestimmung der Stoffübergangskoeffizienten, die für die Beschreibung der SiO_2-Verminderung und Al_2O_3-Erhöhung maßgeblich sind. Außerdem wurde die Veränderung des MnO-Gehaltes untersucht, wobei ein Gießpulver praktisch MnO-frei war. Es hat sich gezeigt, dass die Stoffübergangskoeffizienten mit fortschreitender Zeit bzw. sinkendem SiO_2-Gehalt steigen. Bei dem MnO-freien Gießpulver konnte ein anfänglicher Anstieg des MnO-Gehaltes beobachtet werden, sowie ein darauffolgender Abfall. Zur Interpretation dieser Ergebnisse wurde ein thermochemisches Prozessmodell erstellt. Dabei zeigte sich, dass die Schichtenströmung des Stahls in der oberen Konvektionswalze entlang der Phasengrenze Stahl/Schlacke zu einer Verminderung des Al-Gehaltes führt, wodurch eine Oxidation von Mn möglich wird. Weitere Ergebnisse gestatten die Berechnung der stationären Zusammensetzung und zeigen, dass der stationäre SiO_2-Gehalt nicht null sein kann. Für den hier untersuchten Gießprozess ist eine Verminderung der SiO_2-Reduktion durch einen Mangangehalt des Gießpulvers nicht möglich.

Schüsselwörter: Gießschlacke, SiO_2-Reduktion, Stoffübergangskoeffizient

1. Introduction

This publication deals with compositional changes of continuous casting mold slags associated with the reducing action of aluminum [Al] in the steel. Such changes may occur for sufficiently high contents of [Al], as it is the case for e.g. TRIP steels with < 1.5 mass% Al. Especially an increase of (Al_2O_3) and a decrease of (SiO_2) is observed due to the reaction

$$3\left(SiO_2\right) + 4\left[Al\right] \rightarrow 2\left(Al_2O_3\right) + 3\left[Si\right] \quad (1)$$

H. Harmuth (✉)
Chair of Ceramics, Montanuniversitaet Leoben,
Leoben, Austria
e-mail: harald.harmuth@unileoben.ac.at

Several investigations have already focused on this phenomenon [1–5]. In [1] an exponential change of silica and alumina with time is assumed. In [2] thermodynamic considerations are applied, the authors of [2] conclude that (MnO) can inhibit silica reduction. Kinetic models for the alumina pick-up of the slag are developed in [4] and [5]. In both cases the alumina concentration in the slag pool is represented by an ordinary first order differential equation, which accounts for the feed from the mold powder, the output consumed by the slag film between mold and strand, and the oxidation from the liquid steel. Furthermore in [5] also the absorption of alumina inclusions in the steel is considered. A constant mass transfer coefficient for alumina in the slag is applied, and an analytical solution of the differential equation is therefore achieved easily. The investigations documented in the present paper originate from the fact that a similar model with constant mass transfer coefficient did not show satisfactory agreement with measurements on site. Therefore the following approach was chosen: A model based on differential equations for the species concentrations in the slag was set up for SiO_2, Al_2O_3, and MnO. An inverse evaluation procedure was developed and applied to identify the mass transfer coefficients as functions of the silica content as well as the equilibrium concentrations at the slag/steel interface and a lower limit for the ratios of the mass transfer coefficients in the steel and the slag. To explain the dependency of the mass transfer coefficient on the progress of the silica reduction and [Mn] oxidation observed in the case of manganese free mold powder, further thermochemical modelling was performed.

2. Experiments

The slag pool was sampled for three casting sequences with different mold powders of the compositions shown in Table 1. As the carbon content vanishes before liquefaction, the compositions are represented in terms of oxides and calcium fluoride balanced to 100 mass%.

The steel casted contained approximately 1 mass% Al, >1.5 mass% Mn, and <0.4 mass% Si. Slag specimens have been sampled starting 1 min after the beginning of casting, sampling ended after 50-119 min. During this period relevant process parameters were collected and averaged. Especially mold powder consumption, slag pool thickness, and the cross sectional area of the mold are of importance here. Slab thickness was 215 mm and slab width 1357 to 1457 mm. In Figs. 1a and b, the decrease of silica and increase of alumina content with elapsed casting time are clearly visible.

The progression of the (MnO) content depicted in Fig. 2 is of special interest. Over the whole time period investigated, the (MnO) content is higher for MP1 and lower for MP2 and MP3 compared with the respective original mold powder compositions as shown in Table 1. Therefore it can be concluded that (MnO) is reduced by [Al] for MP2 and MP3, while [Mn] oxidation occurs in the case of MP1. This astonishing behavior will be discussed in Sect. 5.

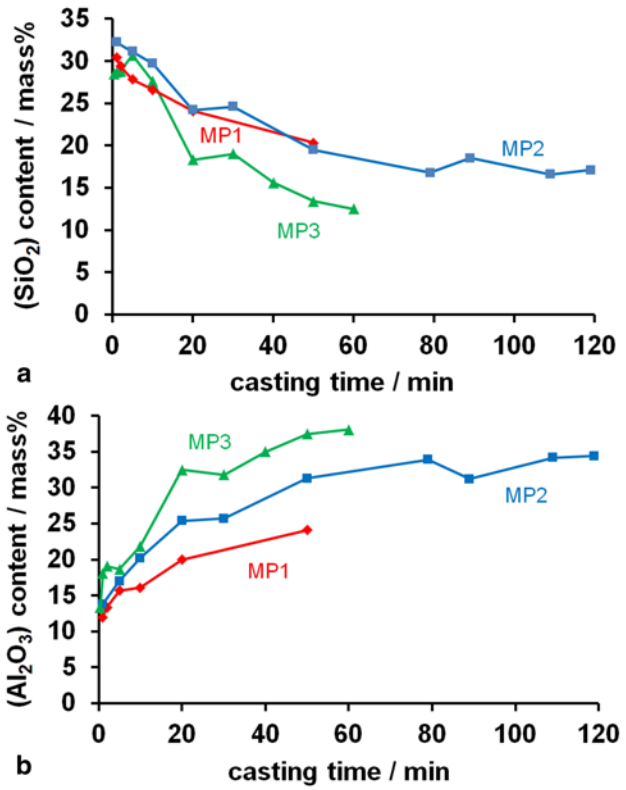

Fig. 1: Decrease of silica content (**a**) and increase of alumina content (**b**) in the slag pool in dependence of elapsed casting time

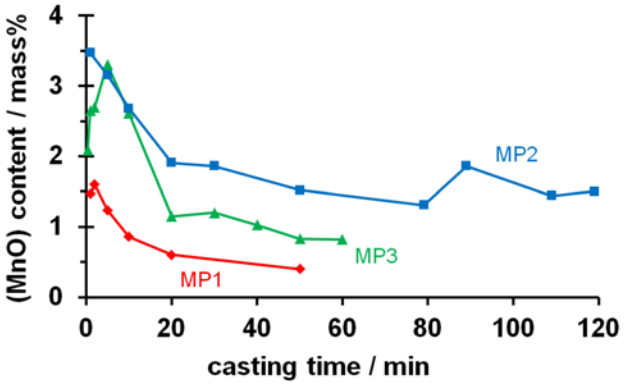

Fig. 2: Dependence of the (MnO) content in the slag pool on the elapsed casting time

3. Modeling Approach and Parameter Identification

A balance of the mass fluxes of the various species entering and leaving the slag pool yields—similarly as applied in [4] and [5]—an ordinary first order differential equation for the concentration c_i of the species i:

$$\frac{dc_0^i}{dt} = -\frac{A}{V_0}\beta_i^{slag}\left(c_0^i - c_e^i\right) + \frac{\dot{V}}{V_0}\left(c_1^i - c_0^i\right) \qquad (2)$$

TABLE 1:
Compositions of mold powders MP1-MP3 in carbon free state represented in terms of oxides and CaF_2 (mass%)

	CaO	CaF_2	SiO_2	Al_2O_3	MgO	Li_2O	Na_2O	K_2O	TiO_2	FeO	MnO	B_2O_3	P_2O_3
MP1	23.4	20.2	37.0	1.75	4.27	0.00	7.66	0.24	0.19	0.38	0.13	3.72	1.01
MP2	7.23	22.1	41.5	4.78	1.34	2.78	12.4	0.58	0.34	0.79	6.05	0.10	0.07
MP3	7.65	23.0	41.1	4.82	1.17	1.90	12.6	0.62	0.08	0.87	5.98	0.21	0.10

Here t is the time, A is the cross sectional area of the mold minus the area covered by the SEN, V_0 is the slag pool volume, $\dot{V}$ the volume flux entering/leaving the slag pool, and β_i^{slag} the mass transfer coefficient of species i in the slag. Furthermore the concentrations c_0^i, c_e^i, and c_1^i refer to the slag pool bulk, the equilibrium concentration in the slag pool at the steel/slag interface, and the original mold flux composition. As preliminary calculations showed that Equ. (2) does not yield satisfactory agreement with measurements, an inverse procedure was established in order to simultaneously identify a variable mass transfer coefficient and the equilibrium species concentration. It was assumed that β_i^{slag} can be represented as a second power algebraic function of $c_0^{SiO_2}$:

$$\beta_i^{slag} = D_0^i + D_1^i \cdot c_0^{SiO_2} + D_2^i \cdot c_0^{SiO_2\,2} \tag{3}$$

Substitution of Equ. (3) into Equ. (2) and integration shows that the coefficients D_k^i can be calculated from a regression analysis:

$$Z_j^i = X_{0,j}^i \cdot D_0^i + X_{1,j}^i \cdot D_1^i + X_{2,j}^i \cdot D_2^i\,; \quad j = 1,\ldots,n-1 \tag{4}$$

Here $j>0$ refers to n-1 of the n particular samples 0,1,...,n-1, n being the total number of sampling times. The quantity Z_j^i and the coefficients $X_{k,j}^i$ received by this procedure are:

$$Z_j^i = c_0^i\left(t_j\right) - c_0^i\left(t_0\right) + \frac{\dot{V}}{V_0}\left(\int_{t_0}^{t_j} c_0^i dt - c_1^i\left(t_j - t_0\right)\right) \tag{5a}$$

$$X_{0,j}^i = \frac{A}{V_0}\left(c_e^i\left(t_j - t_0\right) - \int_{t_0}^{t_j} c_0^i dt\right) \tag{5b}$$

$$X_{1,j}^i = \frac{A}{V_0}\left(c_e^i \int_{t_0}^{t_j} c_0^{SiO_2} dt - \int_{t_0}^{t_j} c_0^{SiO_2} c_0^i dt\right) \tag{5c}$$

$$X_{2,j}^i = \frac{A}{V_0}\left(c_e^i \int_{t_0}^{t_j} c_0^{SiO_2\,2} dt - \int_{t_0}^{t_j} c_0^{SiO_2\,2} c_0^i dt\right) \tag{5d}$$

Here t_0 is the time when sample 0 was taken (1 min after the start of casting), and similar holds for t_j. This means that no information from the first minute was used as conditions are not well defined immediately after the start of casting. Equs. (4) and (5) describe a non-iterative procedure for the determination of β_i^{slag} for the case that c_e^i is known. It was combined with a Newton-Raphson iteration in order to simultaneously identify c_e^i. For this purpose β_i^{slag} received for an iterative approximation of c_e^i was applied to numerically solve Equ. (2), the result was used to calculate the deviation from the measurement in terms of the sum of squared differences, and this error then was iteratively minimized. This procedure results in $c_e^{SiO_2}=0$ for all three mold slags and $c_e^{MnO}=0$ for MP2 and MP3. Further $c_e^{Al_2O_3}$ was calculated for MP2 and MP3 from $c_e^{SiO_2}$ and c_e^{MnO} by considering Equ. (1) and the equivalent relation regarding (MnO) reduction. As an alternative, it was also tested whether $c_e^{SiO_2}$ shows a linear dependence from $c_0^{SiO_2}$ for relatively high (SiO_2) concentrations and vanishes only below a critical value of $c_0^{SiO_2}$. An inverse simulation shows that this critical silica content is larger than the initial one, viz. $c_e^{SiO_2}$ in fact is identical to zero. From this a lower limit for the ratio $\beta_{Al}^{steel}/\beta_{SiO_2}^{slag}$ can be followed. To give an example, for MP1 $\beta_{Al}^{steel}/\beta_{SiO_2}^{slag} \geq 8.47$ was revealed. This is a meaningful result: Only if the ratio quoted above is large enough, a sufficient aluminum supply enables silica reduction being so complete that $c_e^{SiO_2}=0$ is achieved.

4. Mass Transfer Coefficients and Simulation Results

Fig. 3 shows a satisfactory agreement between the simulated and the measured (SiO_2) content in the slag pool for all three mold powders. Deviations mainly show an oscillating character probably due to the fact that only mean values of the process variables have been available. A temporarily higher mold powder consumption at constant feed rate will e.g. transiently decrease the silica content. For MP1 a somewhat larger error occurs for $t>20$ min as all but one measurements have been sampled in the first 40 % of the time period.

Fig. 4 shows the mass transfer coefficients for (SiO_2) and (Al_2O_3) as determined by the procedure explained in Sect. 3. Mass transfer coefficients show a mainly ascending behavior with progressing silica reduction (decreasing silica content). Also for (MnO) mass transfer coefficients can be identified in the same manner for MP2 and MP3, but not for MP1, where [Mn] oxidation can be observed. Therefore these results raise at least two questions: How can the manganese oxidation be explained in the case of MP1, and what is the reason for the increase of the mass transfer coefficients with increasing silica reduction?

5. A Thermochemical Modeling Approach

A thermochemical modeling approach was chosen to answer the questions mentioned above. The relatively

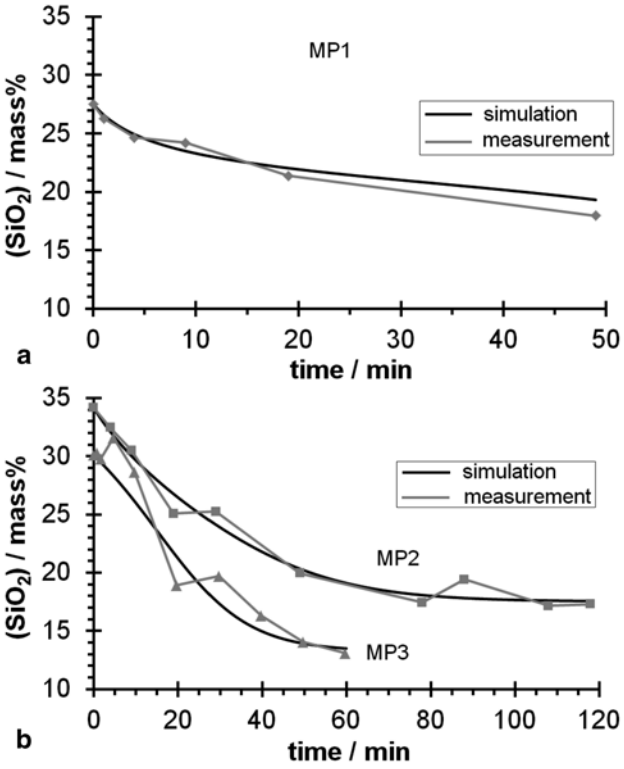

Fig. 3: Simulated versus measured (SiO_2) content for MP1 (**a**) and MP2, MP3 (**b**)

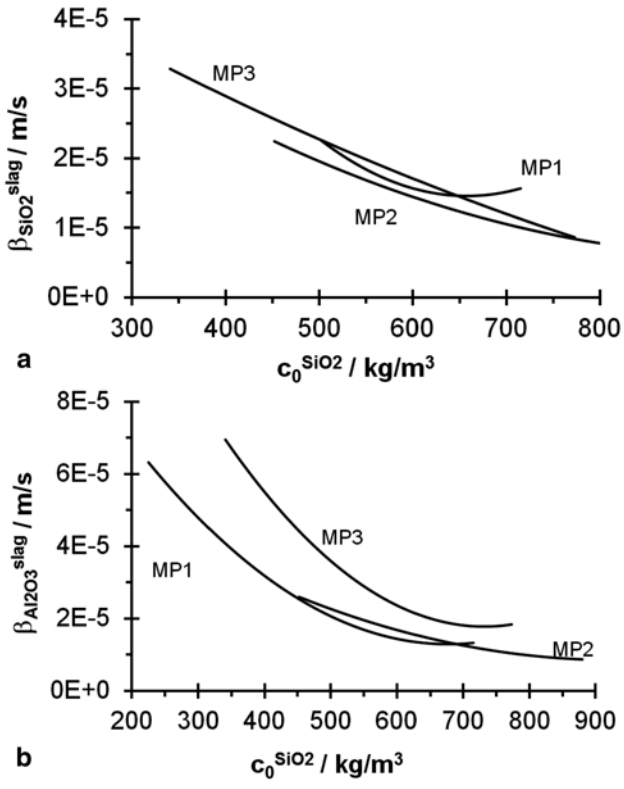

Fig. 4: Mass transfer coefficients in the slag for SiO_2 (**a**) and Al_2O_3 (**b**)

high ratio $\beta_{Al}^{steel}/\beta_{SiO_2}^{slag}$ identified by the inverse evaluation procedure enables $c_e^{SiO_2}=0$ by an excess of [Al] and, out of the same reason, hinders oxidation of [Mn]. Therefore (SiO_2) reduction and [Mn] oxidation must not be expected at the very same location. A possibility for manganese oxidation follows from the flow pattern as it is schematically depicted in Fig. 5a. After leaving the SEN port, a part of the steel flow enters the upper convection roll, impacts the steel/slag interface nearly vertically (which causes a high mass transfer coefficient) close to the mold wall, and then proceeds as a stratified flow parallel to the interface without major intermixture with the residual steel volume. This can be clearly observed from a research work of Thomas et al. [6], especially from an animation shown there.

It is now reasonable that a main part of the reduction processes takes place in the region of the impact flow close to the mold, where steel of original composition is provided and the mass transfer coefficient is relatively high compared to that in the slag phase. The subsequent stratified flow will cause a depletion of [Al] by further reaction with the slag. Then, with decreasing [Al] content, manganese oxidation may become possible in some distance from the mold wall. Therefore two regions should be distinguished at the steel/slag interface: First a reduction zone will occur (cross sectional area A_1), followed by a zone of possible [Mn] oxidation with lower [Al] content (cross sectional area A_2, $A_1+A_2=A$). It should be assumed that A_1 will increase with proceeding silica reduction as less [Al] is consumed. Moreover, mass transfer coefficients calculated as explained above and shown in Fig. 4 have to be regarded to be nominal ones in the light of these considerations: Their calculated values relate to the whole cross sectional area A, but actually reduction with the equilibrium interface concentrations as identified in Sect. 3 takes place in the area $A_1<A$. An increase of A_1 with progressing silica reduction will therefore increase the nominal mass transfer coefficient corresponding to constant A. The special flow pattern associated with the upper convection roll therefore offers an explanation for both the possible [Mn] oxidation and the increase of the mass transfer coefficient with decreasing silica content. To verify these considerations, an effective equilibrium reaction zone model was applied. Details about this technique can e.g. be seen in [7]. The commercially available software FactSage has been used for this purpose, details about the database are explained in [8] and [9]. The kernel of the model structure is schematically depicted in Fig. 5b. The content of reaction zones ([RZ1-4] for steel and (RZ1-4) for slag) is equilibrated and afterwards remixed with the residual volume of the corresponding zones [Z1-4] and the slag pool, respectively. This procedure is iteratively repeated for suitable time steps, while the in- and output of slag and steel are considered according to the process parameters. The reaction zone volumes are proportional to the mass transfer coefficients. As an example for the results Fig. 6 shows the equilibrium contents of [Al] together with (SiO_2) and (MnO), respectively, at the steel/slag interface in dependence of the reaction zone and the time. This calculation was performed for MP2 and the process data observed.

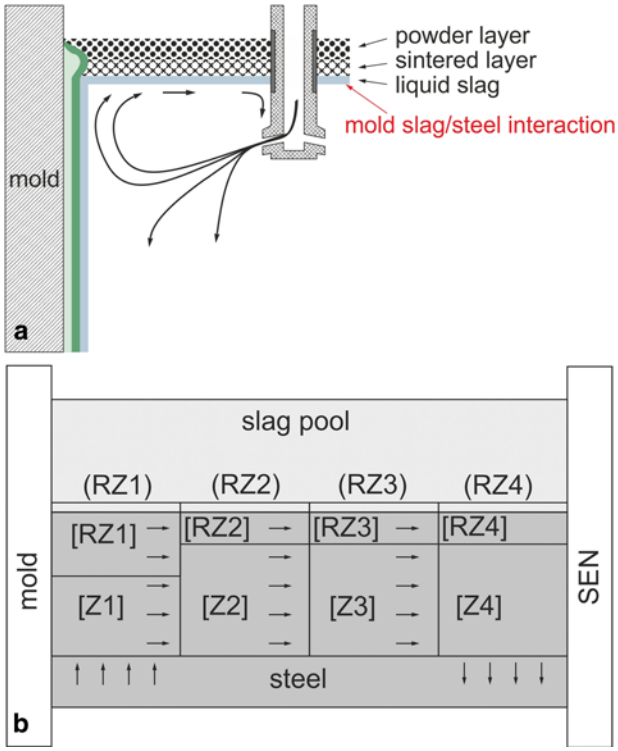

Fig. 5: Schematic representation of the steel flow pattern (**a**) and the reactive equilibrium zone model (**b**) (for explanations see text)

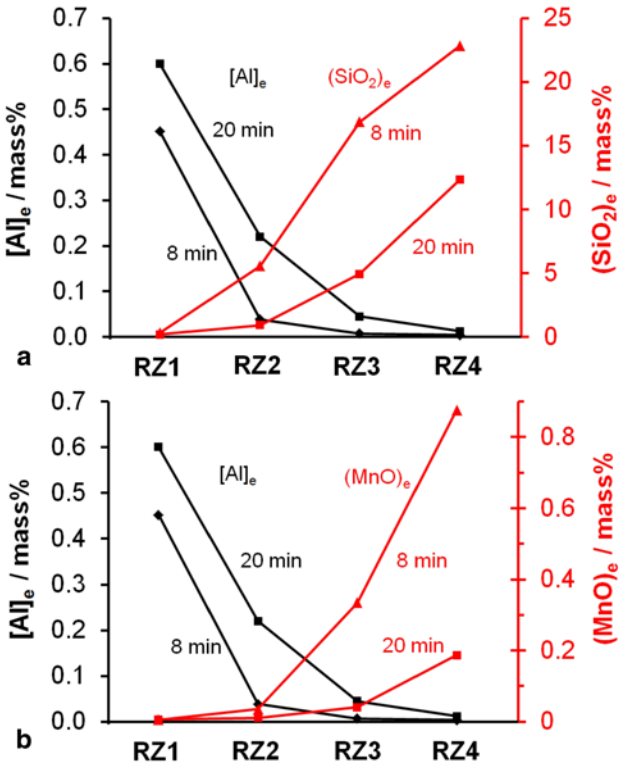

Fig. 6: Equilibrium contents at the steel/slag interface of [Al] together with (SiO_2) (**a**) and (MnO) (**b**) as calculated for MP2 in dependence of the reaction zone and the time

It can be seen that $[Al]_e$ decreases with the reaction zone number and increases with time, whereas $(SiO_2)_e$ increases with the reaction zone number and decreases with time. The content $[MnO]_e$ qualitatively behaves similar as $(SiO_2)_e$. For the following consideration, an arbitrary value of $[Al]_e$ may be fixed as a criterion for the boundary of the reduction zone with area A_1. Then from Fig. 6 it can be seen that this boundary moves in direction of RZ4 with proceeding time. This means an increase of A_1 and a decrease of A_2, and therefore an increase of the nominal mass transfer coefficients. Fig. 7 shows—again for MP2–$(MnO)_e$ in dependence of the silica content in the slag pool and the reaction zone.

Two cases have been investigated. Fig. 7a shows the results calculated for the original mold powder composition containing considerable amounts of MnO. For comparison, a second simulation was performed: The MnO content was canceled in the original composition and the residue again balanced to 100 mass%. The results of this simulation are depicted in Fig. 7b. Both figures also show the MnO content in the bulk of the slag pool (dashed curve). Comparing this with $(MnO)_e$ in the various reaction zones reveals more details about reduction of (MnO) and oxidation of [Mn]. Fig. 7a shows that the (MnO) content in the slag pool is always higher than the equilibrium content. Therefore (MnO) will be reduced in all reaction zones and at any time. A different situation can be seen in Fig. 7b: When the reaction starts at high silica content, [Mn] is oxidized in reaction zones 2–4 and reduced in zone 1 only. With increasing degree of silica reduction and associated increase of the $[Al]_e$ content, reaction zones 2 and 3 switch from [Mn] oxidation to (MnO) reduction, while oxidation continues in zone 4. The different behavior of both investigated cases is reasonable: Only for negligible [Al] contents (viz. not in reaction zone 1), [Mn] oxidation is possible. Then the equilibrium

$$\left(SiO_2\right) + 2\left[Mn\right] \Leftrightarrow 2\left(MnO\right) + \left[Si\right] \tag{6}$$

is decisive. According to the position of manganese and silicon oxidation in the Richardson-Ellingham diagram, this equilibrium will mainly be situated on the left side. Manganese oxidation will be supported by a low (MnO) activity, which is not the case for the original composition of MP2 and for MP3, but for MP1. Moreover, with progressing reaction, not only the increase of $[Al]_e$ but also the decrease of the (SiO_2) activity hinders [Mn] oxidation. Fig. 8 shows the equilibrium contents of (SiO_2) and [Al] at the steel/slag interface again for MP2 in dependence of the silica content in the slag pool. Similarly as in Fig. 7a, reduction occurs in all reaction zones, but predominantly in the first one. The ratio of the contribution of the first reaction zone to the others, especially the second, is decreasing with proceeding silica reduction. The question to be asked is what this means for the areas A_1 and A_2 described above. If A_1 is regarded as a nominal reduction zone with vanishing equilibrium concentration as it follows from the identification procedure introduced in Sect. 3, its size can be chosen so that no further reaction of (SiO_2) takes place

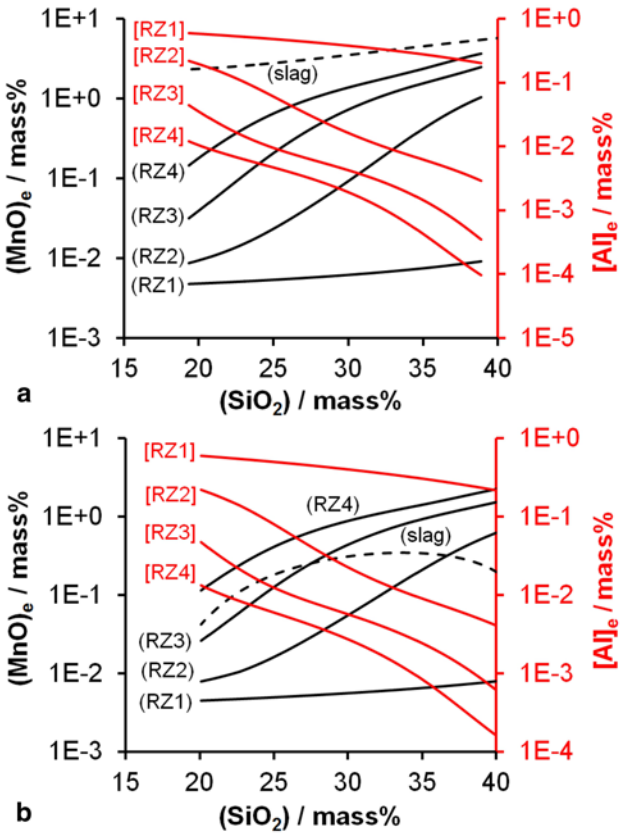

Fig. 7: Equilibrium contents at the steel/slag interface of [Al] together with (MnO) as calculated for MP2 for the original mold powder composition (**a**) and after canceling MnO of the original composition (**b**)

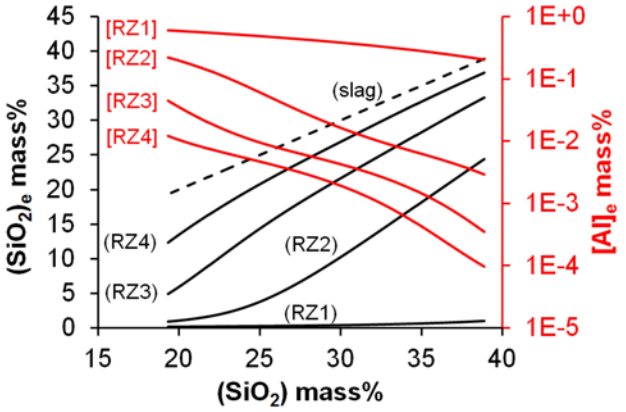

Fig. 8: Equilibrium content of [Al] together with (SiO_2) at the steel/slag interface calculated for MP2

in A_2 and also (MnO) does not react there in the case of the manganese containing slags MP2 and MP3. For the nearly (MnO) free slags (MP1 and MP2, MP3 after canceling MnO), [Mn] oxidation takes place in the area A_2. In both cases A_1 increases with progressing time on the cost of A_2 thus raising the nominal mass transfer coefficient depicted in Fig. 4 with progressing silica reduction.

The simulations described here have also been used to investigate whether a manganese content of the mold powder is able to decrease silica reduction. MP2 was chosen as an example. As canceling the MnO content in the original composition and balancing the residue to 100 mass% increases the silica content, the following procedure was chosen: For the simulation results of the original composition, (MnO) was canceled and all other contents balanced to 100 %. The thus received silica content was compared with that of the simulation with the manganese free composition. It was observed that the ratio of both contents differs from 1 by less than 0.02 for all of the time steps. Therefore it was concluded that manganese content cannot decrease silica reduction at least for the process reported here. The reason can be seen in a comparison of $[Al]_e$ in the reaction zones for both cases: These are nearly identical. This means that the relatively high values of the mass transfer coefficient and the aluminum content in the liquid steel cause an abundance of aluminum compared to (SiO_2) and (MnO) so that the MnO addition is not effective.

6. Discussion of Results and Conclusions

Two modeling approaches have been applied here. The first one presented in Sect. 3 simplifies the model structure so that all necessary parameters can unambiguously be identified by the inverse evaluation procedure established. For the sake of this uniqueness, a further division of the slag/steel interface into an area A_1 where reduction processes occur and a residual area A_2 as explained above was not performed with this model: For (MnO) reduction and [Mn] oxidation, this would lead to the equation

$$\frac{dc_0^{MnO}}{dt} = -\frac{A_1}{V_0}\beta_{MnO,1}^{slag}\cdot c_0^{MnO} + \frac{A_2}{V_0}\beta_{MnO,2}^{slag}\left(c_e^{MnO} - c_0^{MnO}\right) + \frac{\dot{V}}{V_0}\left(c_1^{MnO} - c_0^{MnO}\right) \quad (7)$$

The three addends on the right side of Equ. (7) represent—from left to right—the (MnO) reduction in the area A_1, the [Mn] oxidation in the area A_2, and the difference between (MnO) input to and output from the slag pool. Here it would be necessary to identify both mass transfer coefficients $\beta_{MnO,1}^{slag}$ and $\beta_{MnO,2}^{slag}$, the area A_1, and the equilibrium concentration in the oxidation zone c_e^{MnO}. This is not uniquely possible with the experimental results of Sect. 2 only. Nevertheless the model explained in Sect. 3 is well suitable for identification and simulation of all processes with the exception of [Mn] oxidation in the case of practically manganese free mold powders. Mass transfer coefficients received are regarded to be nominal ones, viz. they are mean values relative to the whole cross sectional area A (and not A_1). Alumina increase can be simulated by the identified mass transfer coefficient shown in Fig. 4b or alternatively by simulating the silica and manganese oxide content and calculating the alumina content stoichiometrically according to the respective redox reactions. A possible difference between both methods may be attributed to alumina nonmetallic inclusions. There was nearly no difference for MP1 and MP2, but alumina content calculated from (SiO_2) and (MnO) was somewhat lower than the

TABLE 2:
Steady state contents of SiO_2, Al_2O_3, and MnO for MP2 and MP3 (mass%)

	SiO_2	Al_2O_3	MnO
MP2	17.5	34.9	1.6
MP3	13.3	39.9	0.9

directly simulated or measured one for MP3. The modeling approach introduced in Sect. 5 is suitable to explain both the [Mn] oxidation for manganese free mold powders and the increase of the nominal mass transfer coefficients with progress of the silica reduction. Additionally the change of the slag composition and viscosity with time may also influence the mass transfer coefficient. Moreover this model helps to reveal that a manganese content of the mold slag does not decrease the amount of silica reduction in this case. But this approach has the drawback that the measurements described in Sect. 2 are not sufficient to unambiguously identify all model parameters: Not all individual mass transfer coefficients of the various reaction zones can be identified in a unique manner. From Equ. (2), the steady state concentration can be determined by equalizing the right side with zero. Then it readily follows that the steady state silica concentration in the slag pool cannot be zero as $c_1^{SiO_2} > 0$. Table 2 shows the steady state contents calculated for MP2 and MP3.

For MP1 the steady state could not be determined with sufficient significance as only one measurement for $t > 20$ min was available. The simulation approach of Sect. 3 was further used to quantify the influence of the various parameters on the silica reduction. For this purpose the following procedure was chosen. The silica decrease was defined as the difference of the silica content of the slag pool after 1 min $c_{0,0}$ and after 50 min $c_{0,1}$. The first derivative of this quantity with respect to the various impacting variables was calculated using the model based on Equ. (2). Then the percentage of the variance caused by the respective impacting variables relative to the total variance of the silica reduction was calculated according to Gauss Law of Error Propagation. This yielded that 68 % of the variance is due to the mold powder consumption $\dot{m}$, which is the mass of mold flux necessary per unit time. The dependency of the silica reduction from other variables can be more easily seen when dimensionless quantities are applied. Four of them are sufficient, which are the dimensionless mold slag volume flux $\dot{V} \cdot t / V_0$, the dimensionless mass transfer coefficient $\beta_{SiO_2}^{slag} \cdot t / l_0$, the dimensionless initial concentration $c_{0,0}/c_1$, and the dimensionless silica decrease $(c_{0,0}-c_{0,1})/c_1$. Here c_1 is the silica concentration of the original mold slag entering the slag pool before any reaction. As a fixed time $t = 50$ min was chosen, the composed quantities $\dot{V} / V_0$ and $\beta_{SiO_2}^{slag} / l_0$ can be used instead of the respective dimensionless numbers. For the measurements evaluated here, the following contributions to the variance of the dimensionless silica reduction have then been revealed: 85 % by $\dot{V} / V_0$, 14 % by $\beta_{SiO_2}^{slag} / l_0$, and 1 % by $c_{0,0}/c_1$. From this it can e.g. concluded that measures increasing the mold powder consumption enable a relatively effective restriction of the silica decrease.

7. Acknowledgements

The research program of the competence center "Advanced Metallurgical and Environmental Process Development" (K1-MET) is supported within the Austrian program for competence centers COMET (Competence Center for Excellent Technologies) with funds of the Federal Ministry for Transport, Innovation and Technology, the Federal Ministry of Economy, the provinces of Upper Austria and Styria, the Styrian Business Promotion Agency, of the Tyrol and the Tyrolian Future Foundation.

References

1. Münch, A. C.; Petry, S.; Schulz, K.; Senk, D. G.: Untersuchungen zur zeitlichen chemischen Veränderung von Gießpulvern, in: 21. Aachener Stahlkolloquium, Aachen, 2006, pp 189–200
2. He, S.-P.; Wang, Q.; Zeng, J.-H.; Zhang, M.; Xie, B.: Properties control of mold fluxes for high aluminum steel, Journal of Iron and Steel Research, 12 (2009), no. 21, pp 59–62
3. Klug, J. L.; Heck, N. C.; Silva, D. d. R; Vilela, A. C. F: Mould slag alumina pick-up due to chemical reactions at the metal-slag interface in the continuous casting process, 65th ABM International Congress, Rio de Janeiro, 2010, pp 1973–1980
4. Yu, X.; Wen, G.-H.; Tang, P; Ma, F.-J.; Wang, H.: Behavior of mold slag used for 20Mn23Al nonmagnetic steel during casting, Journal of Iron and Steel Research International, 1 (2011), no.18, pp 20–25
5. Wang, Q.; Qiu, S.; Zehao, P.: Kinetic analysis of alumina change in mold slag for high aluminum steel during continuous casting, Metallurgical and Materials Transactions B, 2012, pp 424–430
6. Thomas, B. Q.; Yuan, Q.; Sivaramakrishnan, S.; Vanka, S. P.: Transient Fluid Flow in a Continuous Steel-Slab Casting Mold, JOM-e (2002), http://www.tms.org/pubs/journals/JOM/0201/Thomas/Thomas-0201.html
7. Ende, M.-A.; Kim, Y.-M.; Cho, M.-K.; Choi, J.; Jung, I.-H.: A Kinetic Model for the Ruhrstahl Heraeus (RH) Degassing Process, Metallurgical and Materials Transactions B, 2011, pp 477–489
8. Jung, I.-H.; Van Ende, M.-A.; Kim, D.-G.: Thermodynamic modeling of the F containing oxide system and applications to refractory corrosion, 12th Biennial Congress on Refractories UNITECR 2011, Kyoto, 2011
9. Jung, I.-H.; Van Ende, M.-A.: Development of a thermodynamic database for mold flux and application to the continuous casting process, 8th European Continuous Casting Conference ECCC 14, Graz, Austria, 2014, pp 1060–1069